ELSEVIER

Journal of Marine Systems 14 (1998) 81–97

JOURNAL OF MARINE SYSTEMS

Simulating large scale transport of suspended matter

J. Segschneider *,[1], J. Sündermann

Institut für Meereskunde, Troplowitzstrasse 7, D-22529 Hamburg, Germany

Received 30 September 1996; accepted 12 May 1997

Abstract

In this paper a Lagrangian numerical transport model is presented that simulates suspended matter concentrations on large scales. The model is based on the velocity fields of a 22-layer version of the 3.5° × 3.5° Hamburg Large Scale Geostrophic OGCM. Here, the model is applied to the transport of resuspended sediment from the hypothetical source of deep sea mining in the eastern equatorial Pacific. The advection and dispersion of an initially concentrated cloud are simulated for a time range of five decades. Three-dimensional time dependent concentration fields, sedimentation rates at the ocean bottom, the residence time of the particles in the water column and the length of their transport paths are presented. The computed sedimentation rates are compared to the natural background values and estimates of possible consequences for the benthic ecosystem are made. Three experiments are described in this paper. The first one simulates the drift of a particle in the conveyor belt over 1850 years. This experiment is performed to test the advection scheme of the transport model and the currents that are simulated with the underlying circulation model. The second and the third experiment simulate the dispersion of resuspended sediment close to the ocean's bottom and the release of tailings from ocean mining close to the ocean's surface, respectively. In the last two experiments the suspended matter cloud is represented by Lagrangian tracers which possess a mass and diameter distribution according to observations. A main result of experiment two and three is that for the near-bottom source of suspended matter, the drift of resuspended sediment is confined to less than 1000 km, whereas the release of tailings into the surface layer may result in basin wide transport of the fine-grained fraction of the material. The residence time (which here is the time between the release of a Lagrangian tracer and its touch-down at the ocean bottom) of the medium-sized particles is 2 to 3 years for the near-bottom source and up to 20 years for the surface release. The computed sedimentation rates are up to five orders larger than the natural background. Thus, the additional particle flux caused by deep sea mining might easily bury the thin layer of food on which the benthic ecosystem feeds. We also compare the computed residence times of the particles within the water column with residence times derived from ^{238}U to ^{230}Th observations. We estimate, that the settling velocity of the particles doubles by scavenging through biogenic particle fluxes and physical particle interactions (which are not included in the model yet). © 1998 Elsevier Science B.V.

Keywords: models; suspended matter; transport; Lagrangian tracer

* Corresponding author

[1] Present address: European Center for Medium Range Weather Forecast, Shinfield Park, Reading, Berks. RG2 9AX, UK. E-mail: ned@ecmwf.int

PII S0924-7963(97)00021-3

1. Introduction

In the mid sixties, the interest for mining of submarine manganese nodules and ore-containing oozes awoke. Studies on the extent and structure of deposits, on collecting technics and feasibility followed. At the same time concerns about the environmental impacts arose (e.g. Geyer, 1981). Besides from direct disturbances of the benthic fauna by, e.g. the nodule collecting system, large amounts of particulate matter are released into the water column. Sediment will be stirred up close to the ocean bottom and the release of tailings might contaminate the water column at any depth from the bottom to the surface. From accidents like pipeline breakages, additional harm to the environmental system may arise at various depths. The planned mining areas cover about 300 000 km^2 per claim and large amounts of sediment, an estimated 50 000 metric tons per day (Thiel et al., 1991) will be resuspended. The additional sediment load may harm the benthic ecosystem if large amounts of particles settle to the bottom where sedimentation rates on the order of one millimeter per thousand years are common (Seibold and Berger, 1982). In this work we investigate the possible consequences of mining activities in the far field of up to several thousands of kilometers off the source. The simulation of the near-field sediment transport is described elsewhere (Jankowski et al., 1996).

Though data from sediment traps deployed in areas of high biological production show a rapid transport of even small particles to the ocean bottom, it can not be excluded that artificially added particles can drift over large distances before resettling to the ground. Evidence for large scale lateral transport of particles in the deep ocean is given by the distribution of the particle-reactive manganese at the sea floor. Dissolved manganese from hydrothermal sources is consumed by bacteria (Weiss, 1977), which sink downwards at a velocity of 10^{-6} m/s and are scavenged by larger particles with settling velocities of about 10^{-3} m/s (Lavelle et al., 1992). The residence time of manganese from hydrothermal vents in the water column as calculated by Weiss (1977) is 51 years. Horizontal distances of more than thousand kilometers are observed for the Mn transport, with concentrations in the sediment still above background values (Edmond et al., 1982). Thus, there is reason to believe that small particles, and dissolved constituents resulting from cracking of the nodules or stirring up of pore water, may stay in the water column for decades. Our long-term investigation evaluates some possible consequences for the benthic environment. German research activities that investigate the environmental consequences of deep sea mining are focussed in the eastern equatorial Pacific, where a disturbance and recolonization experiment has been performed at the ocean bottom by the TUSCH research group (TUSCH being the German abbreviation for "Deep Sea Environmental Protection") at 7°04′ S, 88°28′ W. This area has been named the DISCOL Experimental Area and is further referenced as DEA.

Our global scale computer model treats the sediment concentration in space as a prognostic variable. To allow the almost immediate calculation of the dispersion of pollutants from any oceanic point source on the globe we use three-dimensional velocities computed with a global ocean model to advect the particles. As the required integration times of the model are on the order of decades and even on the order of thousands of years if the application is extended to radioactive waste disposal, we choose the relatively coarse Hamburg Large Scale Geostrophic OGCM (Maier-Reimer et al., 1993) as a base for our calculations.

A description of the observed and simulated hydrology as well and a brief description of the sediment composition in the Peru Bauer Basin is given in Section 2. The model, a test of the transport scheme and the model's constraints so far are described in Section 3, the experiments and the results can be found in Section 4 together with an estimation of the consequences for the ecology of the studied area. Finally, conclusions are given in Section 5.

2. Currents and sediment composition in the Peru Bauer Basin

The location of the German mining claim in the Peru Bauer Basin is shown in Fig. 1. The center of the claim is roughly at 90°W, 10°S. The Peru Bauer Basin is surrounded by the East Pacific Rise (EPR)

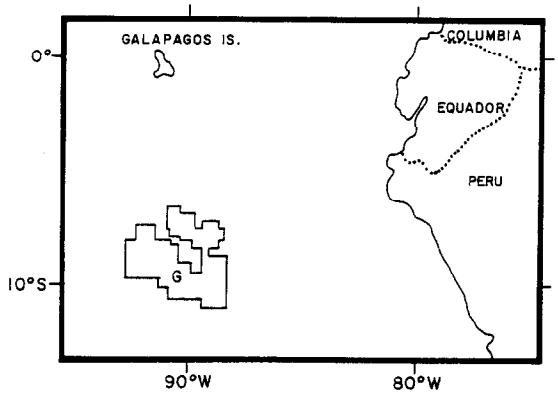

Fig. 1. Location of the German mining claim "G" in the eastern equatorial Pacific. The experimental area DEA is located slightly to the northwest of the claim.

in the west, the Sala y Gomez and the Nazca Ridge in the south, the continental margin of South America with the Peru Trench in the east and the Galapagos Ridge in the north. Sill depths are some 3000 m in the east, 3500 m in the south and 2500 m in the north with several fracture zones in between. The mean depth of the basin itself ranges from 4000 to 4200 m. Lonsdale (1976) reports bottom water inflow into the basin in the southeastern and in the northwestern corner. Above the ridge crest of the EPR, westward flow is predominant at 15°S as can be concluded from δ^3He data collected during GEOSECS (Craig and Lupton, 1981) and more recently by Lupton et al. (1994). Observations of the horizontal current speed that have been obtained with a currentmeter mooring at four depths ranging from 15 m above bottom (mab) to 200 mab at 7°04′S, 88°28′W over a period of two years are analyzed in Klein (1993). The data show a mean flow varying from 0.5 cm/s and 272° at 200 mab to 1.3 cm/s and 307° at 15 mab. The speed is in qualitative agreement with data from Gardner et al. (1984), who observe a mean velocity of 0.5 cm/s in 3671 m depth within the nearby Panama Basin.

The model's current field in the vicinity of the source is presented in Fig. 2. Current vectors are shown for the two lowermost layers in the examined area for January and July. Areas without arrows designate grid boxes in which the ocean is shallower than the layer shown. The assumed source is located in an area of horizontal velocity shear, as eastward currents prevail south of the source and northwestward ones north of it. The deep currents still show seasonal variability in strength and direction. Speeds are generally less than 1 cm/s in the interior of the basin. Higher values of up to 3 cm/s are simulated in areas of flow over submarine barriers. From a comparison with the currents reported by Lonsdale (1976), we find agreement for the direction of the near-bottom inflow into the basin in the northwestern corner. In the southeastern corner of the basin the simulated flow direction is consistent with the observations in July (Fig. 2d) but inconsistent in January,

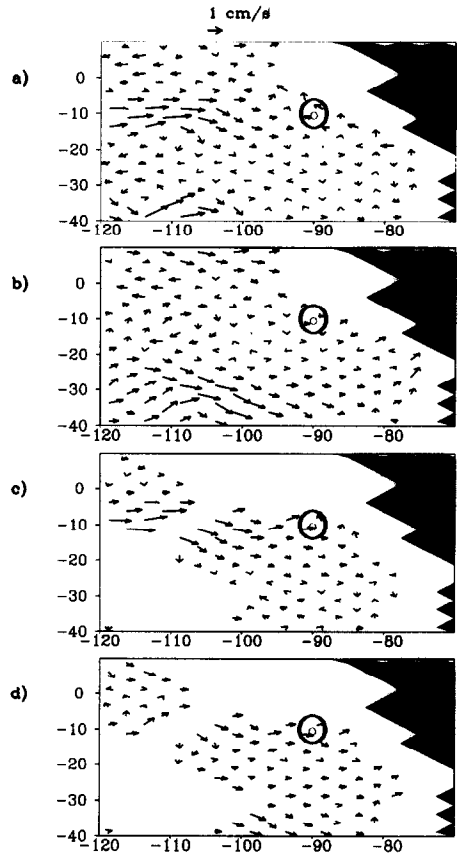

Fig. 2. Horizontal velocities in the two lowermost model layers in the vicinity of the assumed source location (90°W, 10°S). (a) One layer above bottom layer (2956–3419 m), January, (b) one layer above bottom layer, July, (c) bottom layer (3419–3948 m), January, (d) bottom layer, July. The scale vector is on top of (a).

where southward flow is simulated instead of northward flow (Fig. 2c). In the interior, the results are more or less contradictory. Current meter mooring data (Klein, 1993) show relatively strong northwestward currents in the months around January. In one of the two data sets for July a weak southward current is observed and in the other one a strong northwestward current is found, which is preceded by strong southward flow. In the model results at the same position, northwestward currents in January and weak currents in July are simulated with no reliable direction. The observed time series are too short to deduce a seasonal cycle, but it is obvious from the observations and computations that a seasonal cycle resolving model even in the deep sea is more realistic than a model that uses annual means.

With respect to the release of tailings within the water column, the hydrographic state of the upper layers is of interest. No observations have been made near the surface in the DEA. The model's current field in the vicinity of the particle source is shown in Fig. 3. In January a southeastward component is simulated at the source, which extends along the coast of South America, while north of the source location the strong westward equatorial current is predominant. In July, with stronger trade winds, the current is directed off the coast of South America, the velocity being a few cm/s. In the equatorial current, the velocity is up to 80 cm/s in July and slightly less in January. As a consequence of the southward shift of the Inter Tropical Convergence Zone in northern summer eastward flow is found at the northern boundary of the marked domain in July. In the subsurface layer, the equatorial undercurrent is predominant over the whole year with southward extensions along the coast of South America. Velocities are up to 40 cm/s in the undercurrent but do not exceed a few cm/s elsewhere. Due to the eastward flow particulate matter may reach the coast of South America, so that a release of tailings in the surface layers is not advisable.

Strong coastal as well as equatorial upwelling are simulated close to the DISCOL area (Fig. 4). The simulated equatorial upwelling velocities are up to several times 10^{-6} m/s.

The sediment in the Peru Bauer Basin consists of red deep sea clay (Seibold and Berger, 1982) that is rather fine-grained lithogenous material. An investi-

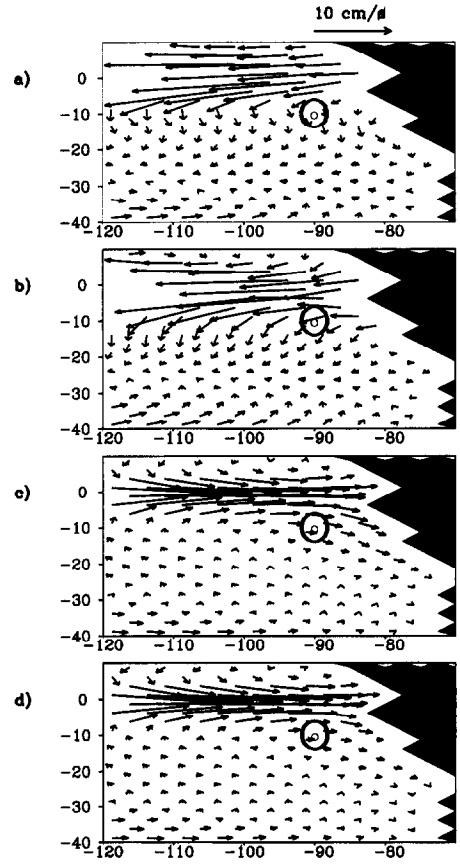

Fig. 3. Horizontal velocities in the two uppermost layers in the vicinity of the assumed source (90°W, 10°S). (a) Surface layer (0–50 m), January, (b) surface layer, July, (c) second layer (50–107 m), January and (d) second layer, July. The velocity scale is on top of (a). Only arrows remaining in the plotted domain are shown.

gation of Schriever of the uppermost centimeter of the sediment in the DEA (published in Klein, 1993; Table 1 in this work) shows that more than 76% of the particles are of 40 μm diameter and less. Following McCave (1975), i.e. assuming a spherical shape of the particles and a 40%/60% in volume composition of organic (density $\rho = 1.03$ g/cm^3) to inorganic ($\rho = 2.5$ g/cm^3) material, the corresponding settling velocity of 76% of the particles is less than 4.2×10^{-5} m/s or 3.7 m/day. For the 40% of the particles that are smaller than 20 μm in diameter, the settling velocity is less than 1.5×10^{-5} m/s, which in turn leads to drifting distances of more than 66.4 km within the time t_{100} required to sink 100 m if a

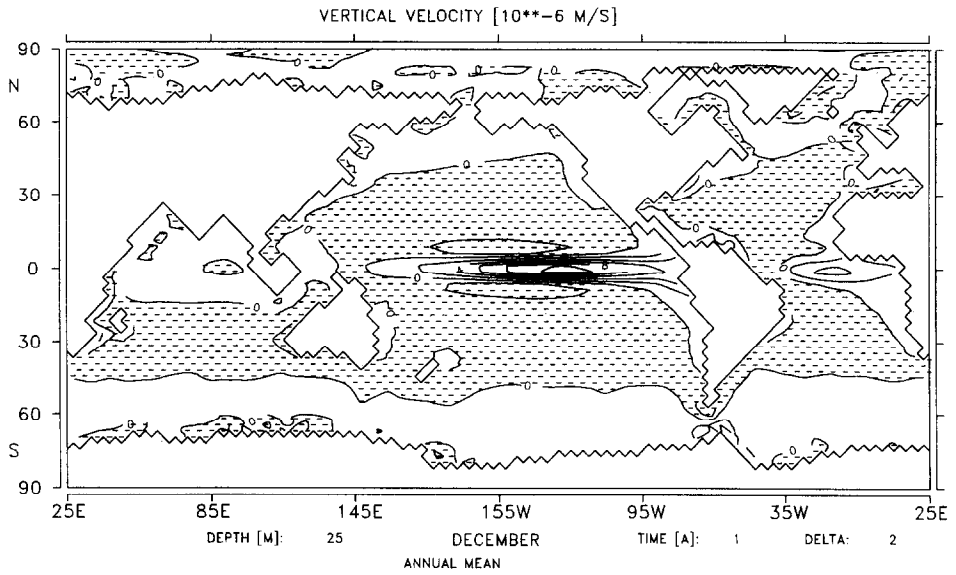

Fig. 4. Annual mean vertical velocity at 50 m depth as computed by the LSG model. The contour interval is 2×10^{-6} m/s. Plain areas indicate upward, shaded areas downward flow.

mean horizontal velocity of 1.5 cm/s is assumed (Klein, 1993).

3. Model features and constraints

A detailed description of the Large Scale Geostrophic (LSG) ocean circulation model is given in Maier-Reimer et al. (1993). The horizontal resolution is 3.5° × 3.5° on an Arakawa E-grid, resulting in a distance of about 500 km between individual grid points. In the model version used for our calculations, the number of layers is 22 with lower boundaries at 50, 107, 172, 246, 330.5, 427, 536.5, 661.5, 804.5, 967, 1152, 1363.5, 1604.5, 1879, 2192, 2549, 2956, 3419.5, 3948.5, 4551.5, 5238.5 and 6000 m. The model is run to steady state for the deep ocean circulation, and is tested with biogeochemical tracers (Maier-Reimer, 1993). Though the model's topography does not resolve the oceanic ridges in their full height, the enclosed structure of the Peru Bauer Basin is preserved. Monthly values of horizontal and vertical velocity, convective overturning and the topography are stored from the circulation model to drive the transport model.

Table 1
Class names, frequency, mass m per particle and settling velocity w_s depending on the particle diameter d according to McCave (1975) and the time t_{100} required to sink 100 m for six sediment classes of the uppermost centimeter of sediment in the DEA

Class	Frequency (%)	d (μm)	m (g)	w_s (m/s)	t_{100} (d)
a	14	100	5.51×10^{-7}	1.6×10^{-4}	7.2
b	3	60	1.21×10^{-7}	7.8×10^{-5}	14.8
c	7	40	3.63×10^{-8}	4.2×10^{-5}	27.5
d	36	20	4.69×10^{-9}	1.5×10^{-5}	77.1
e	20	4	6.20×10^{-11}	1.0×10^{-6}	1157
f	20	0.75	7.80×10^{-13}	1.0×10^{-7}	11574.1

To simulate the transport and diffusion of a dynamical passive tracer, the advection–diffusion equation, i.e.

$$\frac{\partial q}{\partial t} + \sum_i v_i \frac{\partial q}{\partial r_i} - \sum_i \frac{\partial}{\partial r_i}\left(A_i \frac{\partial q}{\partial r_i} \right) = S \qquad (1)$$

has to be solved, where q is the quantity of the passive tracer, v_i are the components of the three-dimensional current vector, r_i the components of the three-dimensional location vector, A_i the exchange coefficients and S the source term of the passive tracer. Here, we use a Lagrangian solution technique for Eq. (1) to avoid the well known numerical prob-

lems of a Eulerian treatment which arise especially in the case of strong gradients of passive tracers (e.g. Gerdes et al., 1991). Furthermore, Lagrangian models allow the direct simulation of transport paths and the computation of residence times. The size distribution of the resuspended particles can easily be taken into account as each Lagrangian particle can have different properties while in Eulerian models usually mean settling velocities are prescribed. Lagrangian transport models have been applied extensively to suspended matter transport in coastal seas such as the North Sea (Maier-Reimer, 1973; Maier-Reimer and Sündermann, 1981; Sündermann, 1993, 1994). Here, the use of the Lagrangian scheme is extended to the global ocean and to particles with a range of settling velocities. Trajectories for an arbitrary number of particles are calculated based on the three-dimensional velocities of the circulation model with a fourth order Runge–Kutta scheme that allows a relatively long time-step of 30 days.

To verify the ocean model's currents on a global scale and to test the advection scheme of the transport model, particles are released at arbitrarily chosen locations and their trajectories are computed without explicit diffusion. A trajectory of a particle in the conveyer belt is shown in Fig. 5. The initial location is in the North Pacific, the initial depth 25 m. Close to the surface, the particle (or, in this case, interpretation in terms of a water parcel is more applicable) is transported through the Banda Straight into the Indian Ocean from where it enters the Antarctic Circumpolar Current (ACC). It circles around Antarctica nearly twice before it enters the South Atlantic via the cold water path, which is the main path for closing the global thermohaline circulation (Rintoul, 1991). After about 500 years the particle enters the Sargasso Sea and becomes part of the Gulf Stream system. After about 1000 years it becomes part of the deep western boundary current and drifts southward, slowly approaching the ACC at greater depth. Finally the particle enters the Pacific again, where it rises due to the weak upwelling in the interior of the Pacific and drifts eastward, still below the surface layer. After 1850 years the cycle is almost closed and the calculation is stopped. The path shown is just one out of many that are possible, and the start location for investigating the conveyor belt would rather be expected in the North Atlantic. However, for the purpose of testing, it strengthened our confidence in both the current field and transport

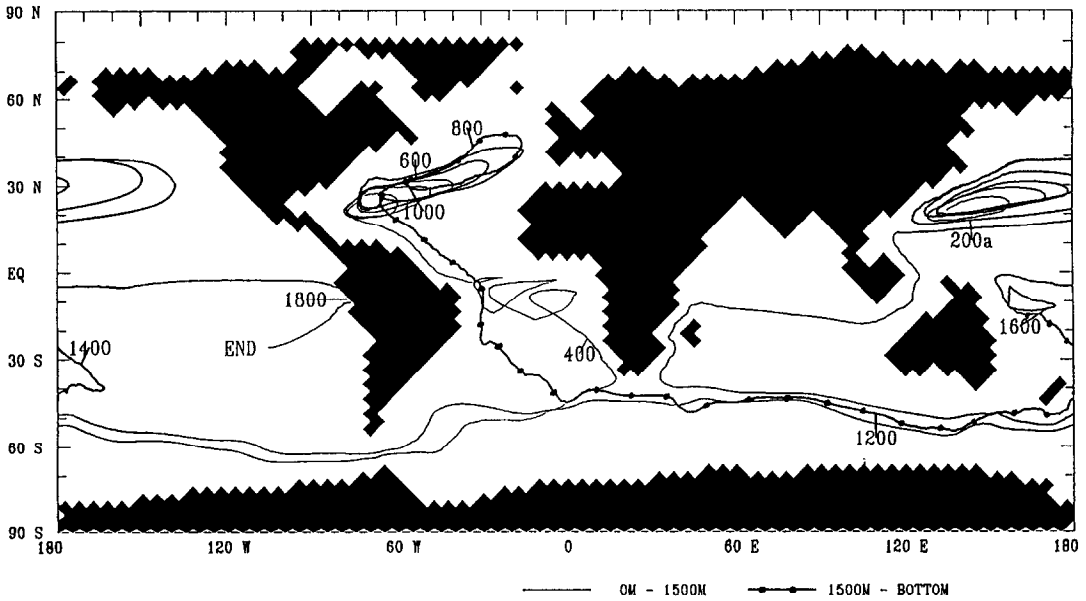

Fig. 5. Particle trajectory after 1850 years. The particle is released in the northwest Pacific off Japan. The numbers along the trajectory denote the drift time in years. The particle is at a depth greater than 1500 m where dots mark the trajectory and between the surface and 1500 m depth elsewhere.

model as the time needed to complete the loop is comparable to the timescale of the thermohaline circulation derived from radiocarbon dating. From the difference of $\Delta^{14}C$ between surface waters in the North Atlantic ($\Delta^{14}C = -50‰$) and mid-depths waters in the Pacific ($\Delta^{14}C = -240‰$) of 190‰ (Broecker and Peng, 1982) and an age : $\Delta^{14}C$ ratio (determined by the radioactive decay time of ^{14}C) of 80 years per 10‰, an overturning time of 1700 years is derived, which is in good agreement with our number, though the simulated particle's cycle is not fully closed. A more detailed study of the simulation of the drift of Lagrangian particles in the conveyor belt can be found in the work of Drijfhout et al. (1996).

For solving the advection–diffusion Eq. (1) the examined system can be divided into two subsystems that are separated by the timescale of their fluctuations (Einstein, 1905; Taylor, 1921; Hasselmann, 1976). The advecting currents of the circulation model represent the slowly varying part, whereas the diffusive term, that is formed by randomly distributed and fast changing turbulent velocity contributions, describes the short scale subsystem. For such a system, the probability p to find a particle at location r at time t is determined by a Fokker–Planck type advection–diffusion equation (e.g. Hasselmann, 1976),

$$\frac{\partial p}{\partial t} + \sum_i \frac{\partial}{\partial r_i}(\bar{v}_i p) - \sum_i \frac{\partial}{\partial r_i}\left(A \frac{\partial p}{\partial r_i}\right) = 0 \qquad (2)$$

where $\bar{v}_i$ are the components of the mean velocity over the ensemble of particles and A is a diffusion coefficient. While investigating Brownian motion, Einstein (1905) showed that A can be expressed as $\frac{1}{2}(\partial\sigma^2)/(\partial t)$, which in the case of stationary turbulence $((\partial\langle v'\rangle)/(\partial t) = 0$, where $\langle v'\rangle$ is the ensemble average of the turbulent velocity v'), reduces to $\sigma^2/2t$. The variance σ^2 of the small scale velocities is given by

$$\sigma^2(t) = \frac{1}{N}\sum_{n=1}^{N}\left[r_i(t) - \bar{r}_i(t)\right]^2 \qquad (3)$$

where N is the number of particles and $\bar{r}_i$ the mean position of the particle ensemble. The position r_i of the single particle along its trajectory at time T is determined by its initial location r_{i_0}, and by the displacements due to advection and turbulence:

$$r_i(T) = r_{i_0} + \sum_{t=0}^{T} \bar{v}_i(r_i,t)\Delta t + \sum_{t=0}^{T} b_i v_i'(r_i,t)\Delta t \qquad (4)$$

where the small scale velocity fluctuations v_i' are taken randomly out of the interval $[-0.5, +0.5]$ and scaled by a bandwidth b_i. The total diffusion of the particle cloud is then determined by relative diffusion, i.e. the randomly fluctuating small scale velocities, and the dispersion of the cloud that is caused by the velocity shear of the large scale circulation, i.e. the ocean model's currents. As only the dispersion of passive tracers is calculated with the model, no feedback mechanisms between the two subsystems in Eq. (2) have to be considered. The velocity fluctuations in the diffusive term in Eq. (4) are top-hat distributed in our model. It can be shown by use of the central limit theorem that for a large number of realizations (i.e., numerical time-steps) the resulting distribution of the particles in space is Gaussian, where "large" is on the order of ten (see, e.g., Hammersley and Handscomb, 1964). The central limit theorem theoretically requires an infinite number of particles, but it has been shown that it works for particle numbers in the order of 10^4 in practical applications (Maier-Reimer, 1973).

The dependence of the exchange coefficient on the maximum diffusion velocity $v'_{i\max}$, is given by (e.g. Csanady, 1973)

$$A_i = \tfrac{1}{6} v'^2_{i\max}\Delta t \qquad (5)$$

with

$$v'_{i\max} = \frac{b_i \Delta x_i}{\Delta t} \qquad (6)$$

where Δx_i are the distances between two grid points in the ith direction, and Δt is the model's time-step. The relation between exchange coefficient and bandwidth then reads

$$A_i = \frac{1}{6}\frac{b_i^2 \Delta x_i^2}{\Delta t} \qquad (7)$$

The approach of Taylor (1921) leads to $A_i = v_i' T_{\mathrm{L}i}$ for long time integrations ($T \gg T_{\mathrm{L}}$), where T_{L} is the

Lagrangian integral timescale (also called decorrelation time), i.e. the time after which subsequent random movements of a particle are statistically independent. In our model this is the case between two time-steps, i.e. $T_L = 30$ days.

A discussion mainly of the vertical eddy exchange coefficient can be found in Gargett (1984). We use a constant value of 10^{-4} m^2/s for the vertical exchange coefficient in our work. Okubo (1971), basing on surface drifter experiments, showed the dependence of the horizontal exchange coefficient on the length scale. For a length scale of 500 km the observed exchange coefficient for relative diffusion is about 1000 m^2/s. This value is commonly used in large scale ocean circulation models (e.g. Cummins, 1991) to parameterize subgrid scale turbulent diffusion. We have chosen the same constant value. In the deep ocean, except close to the bottom where friction effects become important, the exchange coefficient is thought to be smaller than at the surface, as the generally weaker currents imply reduced turbulent velocity shear and hence diffusion. In the DEA, coefficients for horizontal diffusion have been evaluated by Klein (1993) from data obtained with a current meter mooring that worked over a period of two years. The calculated values of the horizontal exchange coefficient as a mean over the two years range from 210 m^2/s at 50 mab up to 710 m^2/s at 15 mab. In a study of the near-bottom dispersion from a radioactive waste dump site done by Kupferman and Moore (1983), a value of 500 m^2/s was used. Though there is evidence for spatial variability of the exchange coefficients, we considered the assumption of constant exchange coefficients representing mean conditions to be more reliable than the use of plausible but uncertain variable values. One more constraint of the model is the neglect of the benthic boundary layer (BBL). As the BBL has a vertical extension of less than 100 m and the major focus of this study is to describe the far field of the sediment cloud, no special assumptions for the velocity in the BBL are made in our model. Compared to the geostrophic layers above the BBL, we assume no large scale lateral transport within the BBL due to the lower horizontal velocities close to the ocean bottom.

Resuspension of sediment from the ocean bottom is not included in the model calculations. Assuming the commonly used relation of the friction velocity u_* to the geostrophic velocity at the upper boundary of the BBL, i.e. $u^* = \frac{1}{30} u_{geostr}$, the critical value of the geostrophic velocity required for resuspension is 30 cm/s, corresponding to a friction velocity of 1 cm/s. In the data of Klein (1993), peak velocities range from 17.1 cm/s at 200 mab to 14.7 cm/s at 15 mab, which seem to be less than needed for resuspension. This is in agreement with results from Bacon and Rutgers van der Loeff (1988) who observed only low concentrations of suspended matter in the eastern equatorial Pacific, indicating no development of a nepheloid layer, which, in turn, they found to be fed by local resuspension rather than lateral transport of suspended matter from the continental slopes.

Biological effects influencing the mean settling velocity, in particular scavenging and flocculation are not considered in the model calculations mainly for two reasons. First, even in areas of high biological production, the observed flux of biogenic matter hardly exceeds 100 mg/m^2 per day (Honjo et al., 1982). Even if a density of only 1 kg/m^3 is assumed for the biogenic particles, it would require 10^6 days to sweep the water column totally. The second reason is that, at least for near-bottom release of sediment, due to the lack of light no phytoplankton will grow and hence no secretion is produced to stick the particles together. Whether the marine snow from near-surface algae blooms has additional potential to scavenge smaller particles is unknown. Also, the production of marine snow and fecal pellets is thought to be rather discontinuous in space and time. Finally, the particles from the deep sea bed have already been part of the food chain and thus should be less attractive for marine organisms due to reduced nutrient content. The red clay that forms the major part of the sediment in the examined area is lithogenous and thus no reason is obvious why it should be attractive for the biota. Apart from biological effects, the particle size and hence settling velocity is affected by the physical interaction of particles, i.e. collisions that cause the growth of larger aggregates. The number of collisions depends mainly on the particle concentration itself. It is caused by small scale Brownian motion (McCave, 1984) which, as long as the additional particles do not change the density of the water significantly, does not depend on the actual

concentration. The aggregation of particles is determined by the number of collisions and the efficiency with respect to subsequent accumulation of the particles.

For artificial seawater and estuarine sediment, the efficiency is assumed to be 0.1 (Edzwald et al., 1974), i.e. 10% of collisions lead to subsequent aggregation. As the release of tailings changes the concentration of suspended matter while the Brownian motion is not affected (at least at some distance from the source), the formation of larger aggregates should be enhanced. However, the processes that determine physical coagulation are investigated mainly for organic matter and mainly to understand the vertical flux of biogenic material during algae blooms (see Alldrege and Jackson, 1995). As the sediment in the Peru Bauer Basin consists mainly of red clay (e.g. Seibold and Berger, 1982), it is not a priori clear whether and how the coalescence efficiency of the resuspended particles is comparable to that of organic material. The role of transparent exopolymer particles in sticking particles together has been discussed recently (Alldrege and Jackson, 1995) and is thought to be of major importance for the build-up of aggregates. To transfer the results from organic to inorganic particles, some questions have yet to be answered, e.g. how the stickiness of the resuspended particles compares to those sinking to bottom from the ocean's surface and how the composition of organic to inorganic material affects the coalescence efficiency. With respect to the latter, it seems plausible that it should be higher for more organic, i.e. less dense and hence softer particles than for more inorganic particles.

Differential settling is one more physical mechanism that causes particle coalescence. It requires the sinking of larger particles from the surface to the bottom. Due to their high settling velocities, the larger particles fall onto smaller and slower ones and the possibility is given that the particles stick together. In the examined area that is not located in the rather narrow equatorial zone of high biological production the loading of the water column with larger particles is observed to be low (Thiel et al., 1991).

On the other hand, macroaggregates may be destroyed by physical forces. One of the processes that disaggregates particles on very small scales is turbulence, which is thought to destroy larger aggregates by raising the velocity of the particle against the viscosity of the water (McCave, 1984). For particles that are larger than the Kolmogorof length,

$$\lambda = \left(\frac{\nu^3}{\epsilon} \right)^{1/4} \tag{8}$$

where ν is the kinematic viscosity of the water and ϵ the dissipation rate of turbulent energy, the velocity shear may cause destruction of the aggregates by shear forces. With a typical value of $\lambda = 5$ mm in the deep sea, this mechanism is of no importance for our much smaller particles. The fast settling of larger fractions may also destroy marine snow aggregates that are rather fragile (Alldrege et al., 1990).

A detailed modelling of the biological and physical particle interactions is beyond the scope of this work. A mean lifetime of 7.5 years for the small-sized seston is derived from ^{238}U–^{234}Th measurements by Bacon and Anderson (1982). As the residence time computed with our model is about 15 years for the fine particles, we estimate a factor of two for the increase of the settling velocity due to biological and physical effects.

4. Experimental setup and results

In this section two experiments are discussed. The first experiment shows the spreading and resettling from a near-bottom release of sediment, representing the stirring up of particles during a mining operation. In the second one a near-surface discharge of tailings is simulated. In both experiments the particles have a mass and settling velocity according to the data collected by Schriever (published in Klein, 1993). Table 1 describes the hydraulic properties of the sediment fractions.

One hundred particles per time-step (i.e., per month) are released to simulate a continuous source of resuspended sediment. The hundred particles are distributed in the classes a to f given in Table 1 and thus the distribution is step-like rather than continuous. The 40% of the particles that are of diameter less than 20 μm are splitted into two classes of 20% with diameters of 4 and 0.75 μm and corresponding settling velocities of 1×10^{-6} and 1×10^{-7} m/s, respectively. The latter one is a lower boundary for

particulate matter that occurs in the ocean (McCave, 1975). The choice of the two classes is somewhat arbitrary, as it is not validated by observations. However, according to Seibold and Berger (1982) red clay particles have a diameter of 1 to 4 μm, and, as the sediment in the DEA is mainly red clay, it can at least be assumed that particles with the chosen diameters are part of the released sediment. Data with better resolution of the grain size that may be obtained during planned experiments within the TUSCH group should help to overcome the current lack. For an assessment of the present results it should be mentioned that with higher settling velocity in relation to the particle diameter, the simulated concentrations will become higher close to the source and lower in the far field. The path of the particles in relation to the settling velocity will not change, however, and thus the outer boundaries of the affected area will remain the same. Hereby it is assumed that $w_s = 10^{-7}$ m/s as a lower limit of the settling velocity is still valid.

The source strength is normalized to 1 since the initial amount of sediment released into the water column is yet uncertain. For a single mining operation, values of up to 50 000 metric tons per day are reasonable (Thiel et al., 1991) for the bottom source. For the release of tailings, a value of 4000 metric tons is assumed from a daily nodule requirement of 1000 metric tons and a nodule content of 20% of the mined material. Concentrations are computed by counting particles and summing up their mass in $1° \times 1° \times 200$ m boxes and will be interpreted in percent of the maximum initial concentration. The initial concentration is determined by the total mass of sediment released within a grid box divided by the volume of the grid box, i.e. assuming a homogeneous distribution. The assumed release results in initial concentrations of 494 μg/l for the near-surface source and 6170 μg/l for the near-bottom source. Ichye and Carnes (1981) assume a daily discharge of 1000 metric tons of dry sediment at the surface and compute an additional sediment load of between 200 and 800 μg/l in the far field (100 to 500 km) for the upper 200 m after 185 days. Thus our assumption for the initial concentration seems to be quite reasonable. After 20 years no further particles are started, as this is the expected lifetime of a mining operation. The dilution of the cloud is calculated for a further 30 years, resulting in a total integration time of 50 years.

4.1. Near-bottom discharge

The source of the particles is located at a depth of 500 mab, i.e. at about 3500 m, at 90°W, 10°S, i.e. in the center of the German mining claim. The height above the ocean bottom is chosen to represent an approximate value for the height of the nepheloid layer. In Fig. 6 the computed distribution of the suspended and resettled particles is shown as sum over all model layers after 20 and 50 years integration time, respectively. Most of the large particles settle down at the ocean bottom close to the source due to their high settling velocity, while smaller ones spread away from the source due to advection and diffusion. Consequently, the area occupied by the cloud is larger after 50 years, while the density of the particles in space decreases. The perpendicular lines in the figure arise from the collision of particles with the vertical boundaries of the grid boxes due to their diffusion velocity. This can be interpreted as sedimentation on sloping topography (Csanady, 1973). Another choice would be the addition of a perpendicular velocity component directed inward from the wall, thus simulating a wavelike reflection of the currents. For our investigation of suspended matter transport we found the sedimentation approach more applicable, whereas for dissolved constituents the wavelike reflection choice seems to be more useful.

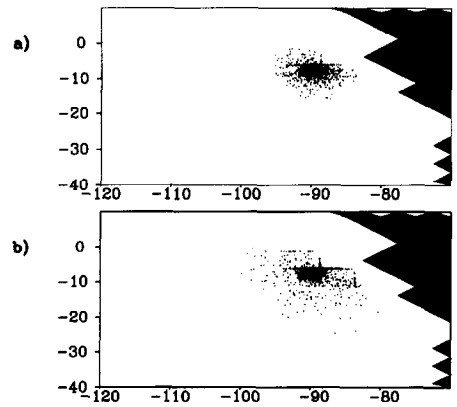

Fig. 6. Horizontal distribution of the floating and resettled particles as sum over all layers for the near-bottom release experiment after (a) 20 years and (b) 50 years integration time.

The calculated concentration fields are shown after twenty years (Fig. 7), i.e. the assumed end of the mining operation, and after 50 years, i.e. at the end of the integration time (Fig. 8). The concentrations are derived by counting the particles per grid box and summing up their mass divided by the volume of the box. The concentration fields after 20 years (Fig. 7a,b,c) show that a large fraction of the released particles are resettling close to the source. Concentrations are up to more than 1000% of the initial concentration, where the initial concentration is given by dividing the amount of particles that are released by the volume of the source grid box. The time that is needed by all but the largest particles to sink through one grid box (i.e., 200 m) is larger than one time step. As new particles are added to the box by the continuous source, concentrations of more than 100% occur. Due to their slow settling velocity, the smaller particles are subject to the advective currents for a longer period. As velocities in the deep sea are low (typically on the order of a few cm/s and less for the geostrophic component) the area affected by the cloud is within some thousand kilometers dis-

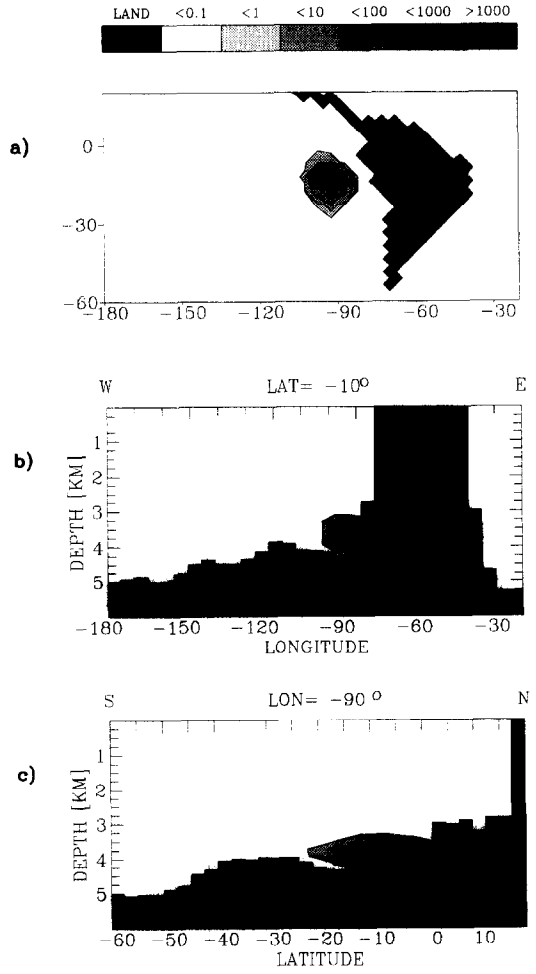

Fig. 7. Concentration in % of initial concentration after 20 years. The source is located at 90°W, 10°S, 3500 m depth. (a) Vertically averaged concentrations, (b) zonal section along 10°S, (c) meridional section along 90°W. Values of more than 100% occur due to accumulation of particles in the respective grid box. The initial concentration is given by the total mass released per time-step divided by the volume of the source grid box. Contour lines are drawn at 0.1, 1, 10, 100 and 1000% of the initial concentration.

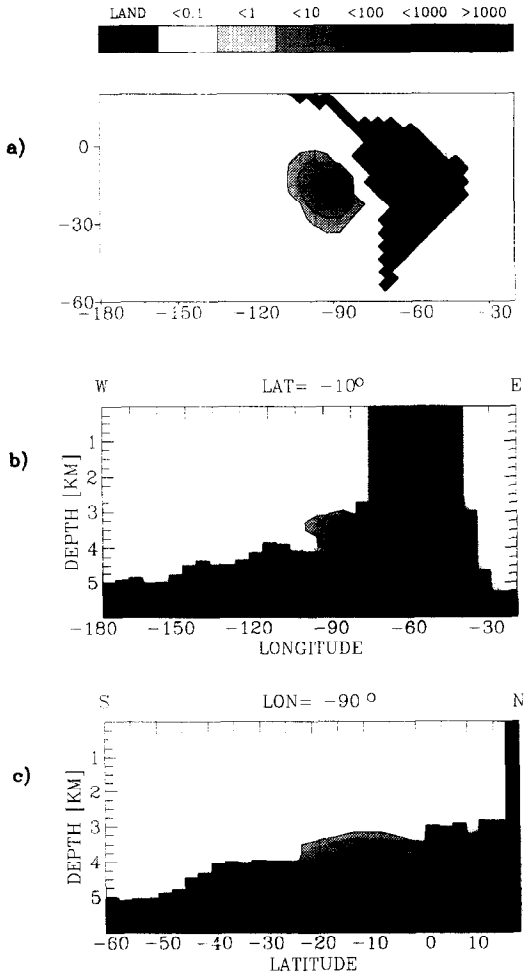

Fig. 8. Same as Fig. 7, but after 50 years integration time.

tance from the source, with concentrations decreasing rapidly towards the boundary of the cloud. The threshold value for the contours is 1‰. Due to the enclosed structure, even the fine-grained material remains in the Peru Bauer Basin (Fig. 7b,c). Thus, for the long time integration, advection becomes less important and diffusion processes result in a more or less symmetrical pattern of the concentration field, with maximum concentrations located at the source point. As the source is assumed to have a lifetime of twenty years, the concentrations in Fig. 7 represent maximum values.

In Fig. 8 the concentrations are shown after fifty years, i.e. thirty years after the assumed end of the mining operation. Consequently, compared to Fig. 7 concentrations decreased and the center of the cloud is slightly shifted southward due to the advecting currents. The extension of the cloud is slightly larger than after 20 years. Maximum concentrations are now within 10%–100% of the initial concentration. From the sections through the cloud we find that vertical diffusion and upwelling are capable of spreading the cloud in the vertical above the sills that surround the basin. While smaller particles are still suspended, larger particles resettle within a few months and thus no longer appear in the water column (Fig. 9).

To estimate the time range and the distance over which the mining operation may endanger the marine ecosystem, it is useful to know how long the particles remain in the water column and how far they drift in that time, see Fig. 9. For calculating the drift distance, the location of the source and the resettling point are stored for every single particle. Particles still floating are not considered. The corresponding distance between start point and resettling point is computed on a great circle whereafter the class distribution for 50 km intervals is counted out. Thus the first bar to the left in Fig. 9a shows the number of particles that drifted between 0 and 50 km, the second the number of particles that drifted between 50 and 100 km and so on. The resulting distribution is Gaussian-like with some skewness due to advection and some irregularities due to the class-like distributed settling velocities. The main part of the particles resettle within 300 km distance of the source.

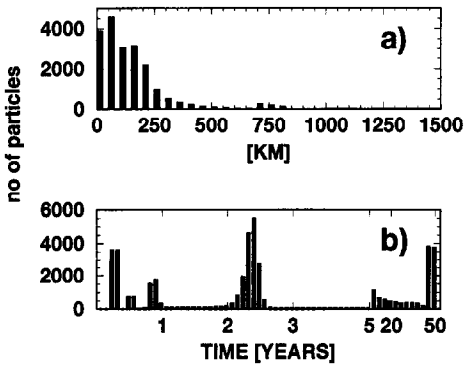

Fig. 9. Number of particles versus (a) horizontal drift and (b) residence time for the bottom release experiment. In (a) the number of particles per 50 km intervals is shown, in (b) the number of particles per month for residence times of up to 5 years and particles per 50 months interval thereafter is shown.

The corresponding residence times, shown in Fig. 9b, reflect the class-like distribution of the settling velocity, as vertical diffusion is much weaker than horizontal. The largest particles (class a, see Table 1) resettle within three to four months, the second largest (class b) within the first year. As the residence time in the water column gets longer, vertical diffusion and the uneven topography smear out the peaks, as can be seen for class c which resettles after two years. After five years the counting interval has been changed to 50 months. It can be seen that particles resettle until the end of the integration time. The large value at 50 years shows the particles still suspended.

The sedimentation rates at various points close to the source are shown in Fig. 10. For the computation of the sedimentation rates in units of mm/year, the source strength is assumed to be 50000 metric tons/day. The resulting sedimentation rates in g per m^2 per year are then converted to mm/year by assuming an average density of 1.5 g/cm^3. Thus a mass accumulation rate of 12.1 g/year is equivalent to an accumulation rate of 81.1 mm/year. This is an increase of about five orders of magnitude compared to the natural background sedimentation rate of about 1 mm per thousand years (Arrhenius, 1963). Although it appears that after 23 years (i.e. 3 years after the end of the mining operation) the major fraction of the resuspended sediment has resettled, Fig. 10b shows that the accumulation rates are still up to 50 times the natural background value, and this

several years after the mining operation stopped. For the last 30 years of the calculation, the sedimentation rates are higher at some distance from the source than directly beneath it as the smaller particles resettle after drift over longer distances.

4.2. Near-surface discharge

Clouds of the floating and resettled particles are shown as sum over all model layers in Fig. 11. After 20 years, the main axis of the cloud is directed to the southeast of the source, with few particles spreading to the west. After 50 years, the southeastern extension of the cloud diminished and the main axis of the cloud is now in the east–west direction.

The resulting concentrations after 20 model years are shown in Fig. 12. While the larger particles quickly sink through the water column, the fine-grained material drifts southeastward with the coastal current and then westward with the westward current that prevails between 20°S and 30°S. Concentrations away from the center of the cloud remain less than 100% of the initial concentration. The sections through 10°S and 90°W (Fig. 12b,c) show almost uniform concentrations within the sinking plume and

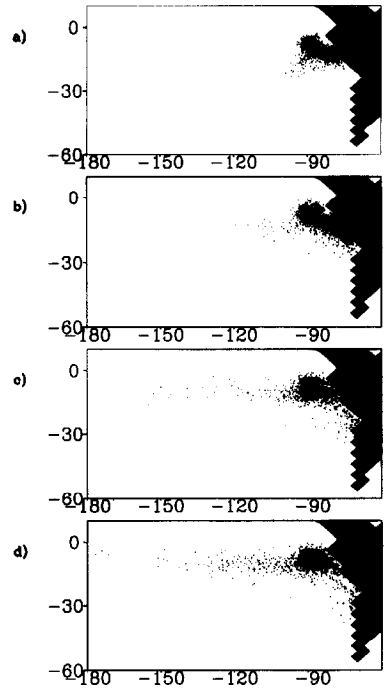

Fig. 11. Distribution of the floating and resettled particles as sum over all layers for the surface release experiment after (a) 10 years, (b) 20 years (c) 35 years, and (d) 50 years integration time.

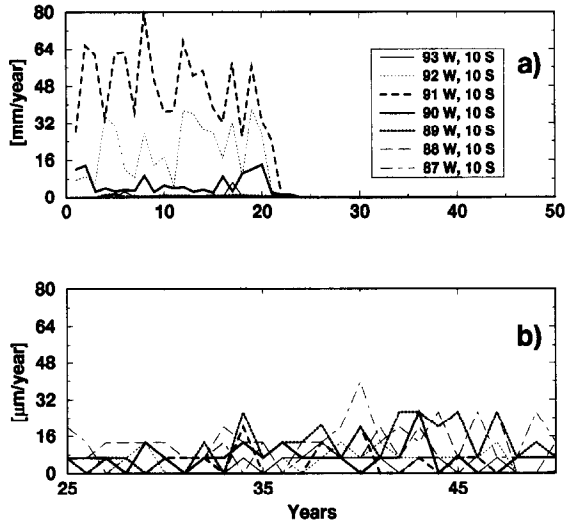

Fig. 10. Time series of the accumulation rates in mm/year of the near-bottom release experiment for various positions close to the source for (a) the whole integration period and (b) the last 25 years (scale blown up). A daily release of 50000 metric tons of sediment is assumed.

sharp gradients at the outer boundary. This is partly due to the coarse resolution of our model, which prevents the large particles from reaching neighboring grid cells within the settling time of approximately two years, the latter being derived by simply dividing the water depth by the settling velocity. After 50 model years only small-sized particles remain suspended and consequently the deeper layers are no longer affected (Fig. 13). This is caused by large equatorial upwelling velocities which are of the same order of magnitude as the settling velocities. So the fine-grained material (smaller than 4 µm in diameter) drifts over distances of thousands of kilometers to the west. The cloud extends to the dateline (Fig. 13a) and its shape is controlled by the westward equatorial surface current. The center of the cloud is still at the source location, where particles are somewhat trapped due to the opposite current directions in the two uppermost layers. This again is an argument against near-surface discharge, especially for the chosen location. Concentrations, how-

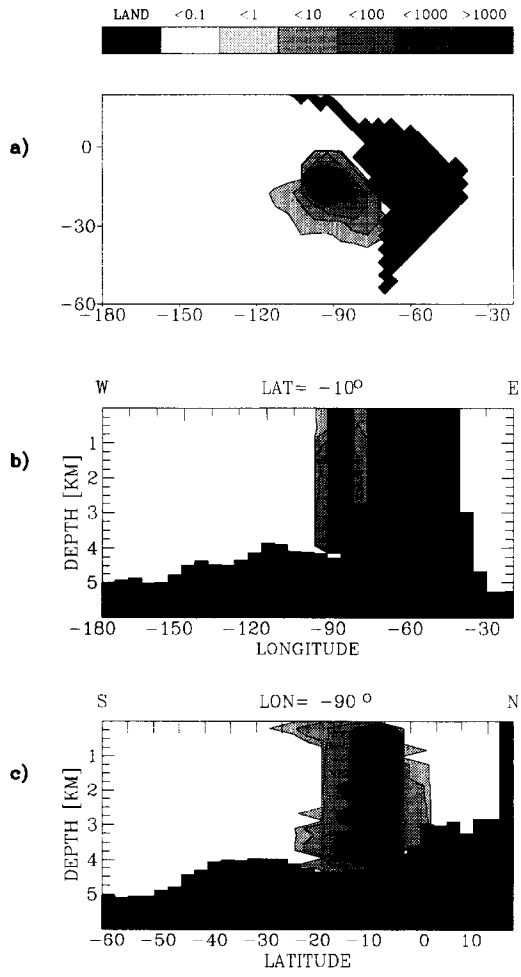

Fig. 12. Concentration in % of initial concentration after 20 years. Source location at 90°W, 10°S, 50 m depth. (a) Vertically averaged concentrations, (b) zonal section along 10°S, (c) meridional section along 90°W. Contour lines are drawn at 0.1, 1, 10, 100 and 1000% of the initial concentration.

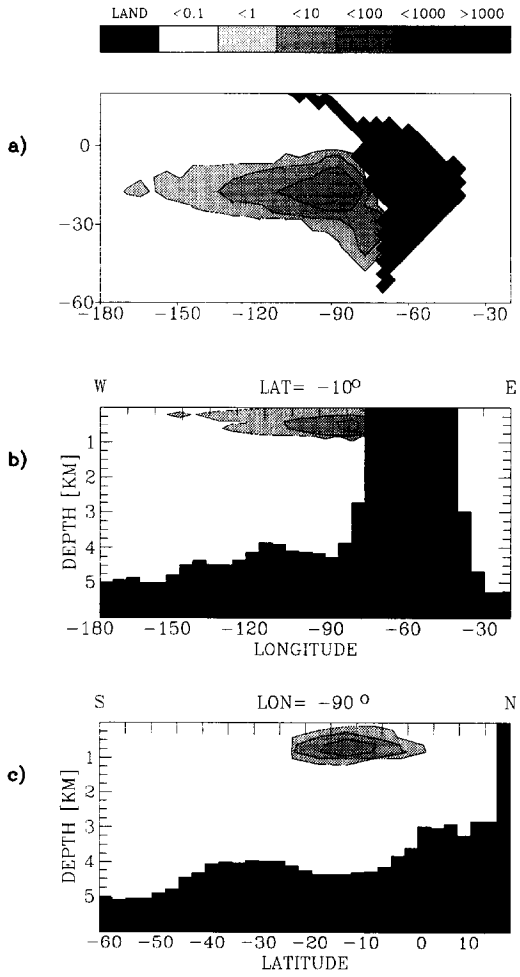

Fig. 13. Same as Fig. 13, but after 50 years integration time.

ever, are only on the order of one percent of the maximum concentrations, due to the small size and mass of the respective particles.

The main part of the suspended matter resettles within 500 km of the source (Fig. 14a). The distribution of the horizontal drift of the particles (Fig. 14a) shows enhanced skewness compared to the bottom release as advection becomes more important due to the longer settling time and higher velocities in the surface layers. As for the bottom discharge, particles

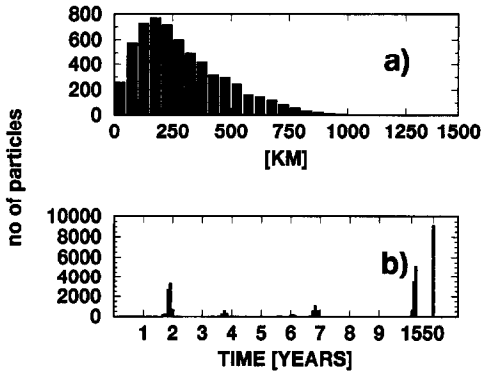

Fig. 14. Number of particles versus (a) horizontal drift and (b) residence time for the surface release experiment. In (a) the number of particles per 50 km intervals is shown, in (b) the number of particles per month for residence times of up to 10 years and particles per 5 year interval thereafter.

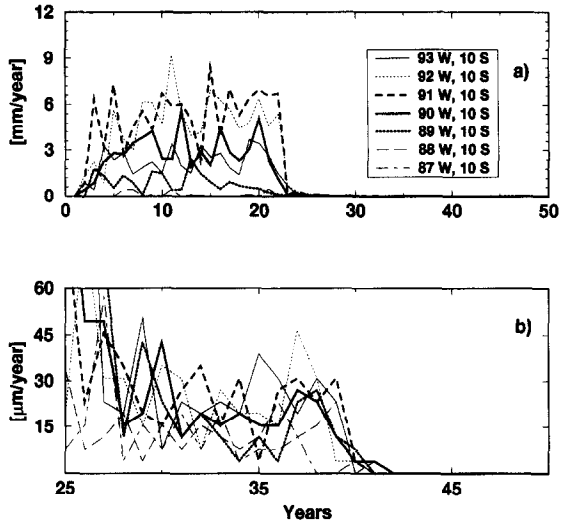

Fig. 15. Time series of the accumulation rate in mm/year for surface discharge at various positions close to the source for (a) the total integration period and (b) the last 25 years (scale blown up). A daily discharge of 4000 metric tons per day is assumed.

still remaining in the water column are not considered here. The maximum of the distribution is in the interval from 150 to 200 km. Exponential decay that approaches zero at 1000 km distance from the source is shown towards larger drifts. The respective distribution of the residence time shows peaks at two years (class a), four years (class b), seven years (class c), and 15 years (class d). The large number for 50 years shows the particles that are still drifting (i.e. the particles smaller than 4 µm in diameter).

Fig. 15 shows time series of the accumulation rates for near-surface discharge. The conversion to accumulation rates in mm/year is made with the same assumptions described in the previous section, except that now a daily discharge of 4000 metric tons is prescribed. Consequently, the rates are lower than for the near-bottom source with maxima between 6 and 9 mm/year close to the source position. These values, however, are still three orders of magnitude larger than the natural background. As Fig. 15b shows, accumulation rates on the order of several µm occur as long as 45 years after the mining operation started, but this will be hard to distinguish from the natural background.

4.3. Estimated influence on ecology

Duce et al. (1991) show the global distribution of the annual inorganic particle flux from the atmosphere to the ocean. The DEA is located in an area of relatively low values of roughly 10–100 mg per m^2 per year. Observations of the suspended matter concentration in the Panama Basin, which is some ten degrees of latitude north of the Peru Bauer Basin, show low suspended matter concentrations of less than 20 µg/kg (Bacon et al., 1989). Observations in the Peru Bauer Basin, that have been made during September and February, did not show phyto-detritus at the sea floor as well as tv-camera pictures did not show macroaggregates in the water column (Thiel, personal communication). Thus it seems likely that biogenic particle fluxes are weak and that the organisms in the examined area are adapted to low suspended matter concentrations. Though it is known that benthic communities depend on the supply of food by sinking organic matter (Pfannkuche, 1993) little is known about the mechanisms of the nutrient uptake in detail. Ozturgut et al. (1981) discuss the growth of bacteria attached to the released particles and the subsequent rise in oxygen demand. A change of the composition of the particles towards more organic and nutrient rich particles can be caused by phytoplankton which feeds on the bacteria, but this would require a long residence time in the euphotic zone. According to the results given in Sections 4.1 and 4.2, the expected near-bottom concentrations are on the order of several hundreds of µg/l, that is about one order of magnitude larger than the observed natural background. The main part of the enhanced concentrations is caused by the larger particles though, and thus it seems unlikely that these will change to more organic ones as their residence time in the upper 100 m is only about 1–2 weeks (Table 1).

With respect to the accumulation of resettling particles at the sea floor, the results show that the simulated accumulation rates are some orders of magnitude larger than the naturally occurring ones. Ozturgut et al. (1981) discuss the burying of food by resettling particles and find that the food is distributed in a rather thin layer, which might easily be buried. Our results imply that this would be the case within some 5° distance of the mining operation

during its active period, and, at some points, even decades after the cessation of the mining operation.

5. Conclusions

A Lagrangian transport model has been developed on the basis of the Hamburg Large Scale Ocean Circulation Model in order to simulate suspended matter transport on a global scale. For the potential particle sources arising from deep sea mining in the Peru Bauer Basin, two scenarios were examined. For the near-bottom source, residence times of the order of months have been calculated for 100 μm particles with corresponding drifting distances of up to one hundred kilometers. For a given settling velocity of 10^{-7} m/s, which is regarded as a lower boundary of the settling velocities occurring in the ocean, residence times are more than fifty years (the performed integration time). The resettling of the sediment cloud is restricted to the enclosed Peru Bauer Basin mainly within 500 km distance of the source. For the surface discharge scenario, resettling takes place within about one thousand kilometers from the source for the larger particles while the smallest ones may disperse westward across the equatorial Pacific. Sedimentation rates for both scenarios are orders of magnitude higher than natural background values. For the benthic ecosystem, the burial of food by the additional sedimentation might cause severe problems.

Acknowledgements

K. Six gave helpful hints for the biological aspects, and S. Beddig helped improving the paper with respect to the English language. This work was sponsored by the German Ministry for Science and Technology (03F0010A, 03G0106D).

References

Alldrege, A.L., Granata, T.C., Gotschalk, C.C., Dickey, T.D., 1990. The physical strength of marine snow and its implications for particle disaggregation in the ocean. Limnol. Oceanogr. 35 (7), 1415–1428.

Alldrege, A.L., Jackson, G.A., 1995. Topical studies in oceanography: aggregation in marine systems. Deep Sea Res. 42, 1–273.

Arrhenius, G., 1963. Pelagic sediments. In: Hill, M.N. (Ed.), The Sea, vol. 3. Interscience, New York, pp. 655–727.

Bacon, M.P., Anderson, R.F., 1982. Distribution of thorium isotopes between dissolved and particulate forms in the deep sea. J. Geophys. Res. 87, 2045–2056.

Bacon, M.P., Rutgers van der Loeff, M.M., 1988. Removal of thorium-234 by scavenging in the bottom nepheloid layer of the ocean. Earth Planet. Sci. Lett. 92, 157–164.

Broecker, W.S., Peng, T.H., 1982. Tracers in the Sea. Lamont–Doherty Geological Observatory, Columbia University, New York, 690 pp.

Cummins, P.F., 1991. The deep water stratification of ocean general circulation models. Atmos. Ocean 29, 563–575.

Craig, H., Lupton, J.E., 1981. Helium-3 and mantle volatiles in the ocean and the oceanic crust. In: Emiliani, C. (Ed.), The Sea, vol. 7. The Oceanic Lithosphere. Wiley, New York, pp. 391–428.

Csanady, G.T., 1973. Turbulent Diffusion in the Environment. Reidel, Dordrecht, 248 pp.

Drijfhout, S.S., Maier-Reimer, E., Mikolajewicz, U., 1996. Tracing the conveyor belt in the Hamburg Large Scale Geostrophic Ocean General Circulation Model. J. Geophys. Res. 101(22): 563, 575.

Duce, R.A., Liss, P.S., Merrill, J.T., Atlas, E.L., Buat-Menard, P., Hicks, B.B., Miller, J.M., Prospero, J.M., Arimoto, R., Church, T.M., Ellis, W., Galloway, J.N., Hansen, L., Jickells, T.D., Knap, A.H., Reinhardt, K.H., Schneider, B., Soudine, A., Tokos, J.J., Tsunogai, S., Wollast, R., Zhou, M., 1991. The atmospheric input of trace species to the world ocean. Global Biogeochem. Cycles 5, 193–259.

Edmond, J.M., von Damm, K.L., McDuff, R.E., Measures, C.I., 1982. Chemistry of hot springs on the East Pacific Rise and their effluent dispersal. Nature 297, 187–191.

Edzwald, J.K., Upchurch, J.B., O'Melia, C.R., 1974. Coagulation in estuaries. Environ. Sci. Technol. 8, 58–63.

Einstein, A., 1905. Über die von der molekularkinetischen Theorie der Wärme geforderte Bewegung von in ruhenden Flüssigkeiten suspendierten Teilchen. Ann. Phys. IV, 549–560.

Gardner, W.D., Bishop, J.K.B., Biscaye, P.E., 1984. Nephelometer and current observations at the STIE site Panama Basin. J. Mar. Res. 42 (1), 207–219.

Gargett, A.E., 1984. Vertical eddy diffusivity in the ocean interior. J. Mar. Res. 42, 359–393.

Geyer, R.A. (Ed.), 1981. Marine Environmental Pollution, vol. 2. Dumping and Mining. Elsevier, Amsterdam, 574 pp.

Gerdes, R., Köberle, C., Willebrand, J., 1991. The influence of numerical advection schemes on the results of ocean general circulation models. Climatol. Dynam. 5, 211–226.

Hammersley, J.M., Handscomb, D.C., 1964. Monte Carlo Methods, Methuen's Statistical Monographs. Methuen, London, 178 pp.

Hasselmann, K., 1976. Stochastic climate models, part I. Theory. Tellus 28 (6), 473–485.

Honjo, S., Manganini, S.J., Cole, J.J., 1982. Sedimentation of biogenic matter in the deep ocean. Deep Sea Res. 29, 609–625.

Ichye, T., Carnes, M., 1981. Sediment dispersion and other environmental impacts of deep-ocean mining in the eastern tropi-

cal Pacific Ocean. In: Geyer, R.A. (Ed.), Marine Environmental Pollution, 2. Dumping and Mining. Elsevier Oceanography Series, 27b, pp. 475–517.

Jankowski, J.A., Malcherek, A., Zielke, W., 1996. Numerical modeling of suspended sediment due to deep-sea mining. J. Geophys. Res. 101, 3545–3560.

Klein, H., 1993. Near-bottom currents in the deep Peru Basin DISCOL Experimental Area. D. Hydrogr. Z. 45, 31–42.

Kupferman, S.L., Moore, D.E., 1983. Dispersion of dissolved tracers released at the seafloor. In: Park, P.K., Kester, D.R., Duedall, I.W., Ketchum, B.H. (Eds.), Wastes in the Ocean, 3. Radioactive Wastes in the Ocean. Wiley, New York, pp. 153-182.

Lavelle, B., Cowen, J.P., Massoth, G.J., 1992. A model for the deposition of hydrothermal manganese near ridge crests. J. Geophys. Res. 97 (C5), 7413–7424.

Lonsdale, P., 1976. Abyssal circulation of the southeastern Pacific and some geological implications. J. Geophys. Res. 81 (6), 1163–1176.

Lupton, J.E., Greene, R., Paradis, G., Urabe, T., 1994. The far-field hydrothermal plume from the southern East Pacific Rise and its relationship to sources on the ridge axis. EOS 75 (44), 320.

Maier-Reimer, E., 1973. Hydrodynamisch–numerische Untersuchungen zu horizontalen Ausbreitungs- und Transportvorgängen in der Nordsee. Mitteilungen des Instituts für Meereskunde der Universität Hamburg, 26, 56 pp.

Maier-Reimer, E., 1993. Geochemical cycles in an ocean general circulation model: preindustrial tracer distributions. Global Biogeochem. Cycles 7, 645–677.

Maier-Reimer, E., Sündermann, J., 1981. On tracer methods in computational hydrodynamics. In: Abott, M.B., Cunge, J.A. (Eds.), Engineering Application of Computational Hydraulics, 1. Pitman Advanced Publishing Program, pp. 198–217.

Maier-Reimer, E., Mikolajewicz, U., Hasselmann, K., 1993. Mean circulation of the Hamburg LSG OGCM and its sensitivity to the thermohaline surface forcing. J. Phys. Oceanogr. 23 (4), 731–757.

McCave, I.N., 1975. Vertical flux of particles in the ocean. Deep Sea Res. 22, 491–502.

McCave, I.N., 1984. Size spectra and aggregation of suspended particles in the deep ocean. Deep Sea Res. 31 (4), 329–352.

Okubo, A., 1971. Oceanic diffusion diagrams. Deep Sea Res. 18, 789–802.

Ozturgut, E., Lavelle, J.W., Burns, R.E., 1981. Impacts of manganese nodule mining on the environment: results from pilot-scale mining tests in the north equatorial Pacific. In: Geyer, R.A. (Ed.), Marine Environmental Pollution, 2. Dumping and Mining. Elsevier Oceanography Series, 27b, pp. 437-474.

Pfannkuche, O., 1993. Benthic response to the sedimentation of particulate organic matter at the BIOTRANS station, 47°N, 20°W. Deep Sea Res. 40, 135–149.

Rintoul, S.R., 1991. South Atlantic interbasin exchange. J. Geophys. Res. 96, 2675–2692.

Seibold, E., Berger, W.H., 1982. The Sea Floor. Springer, Berlin, 288 pp.

Sündermann, J., 1993. Suspended particulate matter in the North Sea: field observations and model simulations. Philos. Trans. R. Soc. London A 343, 423–430.

Sündermann, J. (Ed.), 1994. Circulation and Contaminent Fluxes in the North Sea. Springer, 654 pp.

Taylor, G.I., 1921. Diffusion by continuous movements, Proc. London Mathematical Society, 2 (XX). In: The Scientific Papers of Sir Geofr. Ingman Taylor, Vol. II. Meteorology, Oceanography and Turbulent Flow, 1960. Cambridge, pp. 172–184.

Thiel, H., Foell, E., Schriever, G., 1991. Potential environmental effects of deep sea mining. Report Nr. 26, Zentrum für Meeres- und Klimaforschung der Universität Hamburg, 243 pp.

Weiss, R.F., 1977. Hydrothermal manganese in the deep sea: scavenging, residence time and $Mn/^{3}He$ relationships. Earth Planet. Sci. Lett. 37, 257–262.